PCCP

Accepted Manuscript

ROYAL SOCIETY OF CHEMISTRY

www.rsc.org/pccp

Spectroscopic Study of Ionic Liquid Adsorption from Solution onto Gold

David A. Beattie,[†*] *Sarah L. Harmer-Bassell,*[‡] *Tracey, T. M. Ho,*[†] *Marta Krasowska,*[†] *John Ralston,*[†] *Pasindu M. F. Sellapperumage,*[†] *and Patryk Wąsik.*[†#§]

[†] The Ian Wark Research Institute, University of South Australia, Adelaide, SA 5095, Australia.

[‡] School of Chemical and Physical Sciences, The Flinders University of South Australia, SA 5042, Australia

* Corresponding Author: Email: David.Beattie@unisa.edu.au, telephone number: +61 8 8302 3676

[#] Student on leave from Faculty of Applied Physics and Mathematics, Technical University of Gdansk, Narutowicza 11/12, 80-233 Gdansk, Poland

[§] current address: School of Physics, University of Bristol, Tyndall Ave, Bristol BS8 1TL, United Kingdom

ABSTRACT

Gold was exposed to ethanol solutions containing 0.1 wt. % 1-hexyl-3-methyl-imidazolium bis(trifluoromethanesulfonyl)imide (HMIM NTf_2), an ionic liquid (IL). The resulting adsorbed layers were interrogated using X-ray photoelectron spectroscopy (XPS – both conventional and synchrotron-based) and spectroscopic ellipsometry. Ellipsometry indicated that the adsorbed layer thickness was smaller than the size of an IL ion pair, with an average determined layer thickness of 0.15 nm. This value indicates that the adsorbed layer on gold is most likely patchy. Conventional XPS revealed that the IL adsorbs irreversibly to gold, with equal amounts of anion and cation in the adsorbed layer. High signal-to-noise synchrotron XPS spectra permitted detailed deconvolution of the S 2*p* and N 1*s* peaks for the IL-treated gold, providing more information on adsorbed layer composition and structure. Spectra acquired as a function of X-ray exposure time indicate that non-interacting physisorbed IL components are preferentially removed at the expense of surface bound components, and that anion and cation are both present in the surface bound layer, and also in the layer above. A model structure for the IL adsorbed on gold is proposed.

KEYWORDS. Ionic liquid, adsorption, gold, x-ray photoelectron spectroscopy, ellipsometry.

INTRODUCTION

Room temperature ionic liquids (RTILs or ILs: anion/cation pairs with hindered crystallization) are presently used as lubrication fluids [1, 2] and lubrication fluid additives [3-7], as solvents for the formation of metal nanoparticles [8-12], and as electrolytes in energy storage and capacitors [13-15] (including supercapacitors [16]). In these applications, the interaction of the IL with interfaces is paramount. In lubrication with bulk ionic liquids, there is significant interest in the formation of structured layers immediately adjacent to an interface [17], due to the influence this has on surface forces and friction [18-21]. When used as lubricant additives, their affinity for a metal interface is important in the formation of anti-wear coatings [3, 5]. With energy storage devices and other electrified interfaces, often the critical factor in device/electrode design is the speed with which ILs can wet the electrode material [22-24], especially during the manufacturing process [25]. In the case of nanoparticle formation, the interaction of the anion or cation of the IL with the growing metal nanocrystals is now known to influence the size, shape, and stability of the formed nanomaterials [8, 26].

An understanding of reactivity, binding mechanisms, orientation, and layer structure at solid interfaces is required if ILs are to be selected or designed for these applications (and others), and spectroscopic techniques are most often chosen for this task. In the area of bulk ionic liquids interacting with solid interfaces, significant advances in this area have come from studies using X-ray reflectivity[17], surface enhanced Raman scattering (SERS) [27, 28], and sum frequency spectroscopy [29], although the latter has the most versatility in probing different interfaces (metals, oxides, salts, organic materials). In the area of IL solutions, fewer experiments have been performed, with a limited number of SERS studies [30], ex situ spectroscopic measurements of wear films formed during friction studies [3, 4, 6], and some NMR spectroscopic studies of IL lubricant additive interactions with metals [7].

Conventional XPS has been used extensively to study IL layers on solids (and IL bulk interfaces [31, 32]), and this application of XPS was recently reviewed by Steinrück [33]. Of particular interest for the current work are the papers on XPS of vapor deposited IL on solid substrates. This methodology has allowed the investigation of a number of ILs in sub-monolayer and mono/multilayer amounts on alumina, mica, gold, silver, lithium, and copper [34-38]. However, vapor deposited IL layers may not representative of IL adsorbed from a solvent. We have chosen to probe the surface structure of ionic liquid components adsorbed to a sputtered gold substrate, with adsorption occurring from IL solutions in ethanol. Adsorption thus occurs based on affinity for the metal, and permits removal of the substrate from the immersion solution (and solvent rinsing). Adsorbed films can then be interrogated in the dry state and high sensitivity spectroscopic probes then be used to study the adsorbed layer, with the formation conditions more closely mimicking those of the potential application of ILs in the area of lubrication additives [3, 4, 39]. The reversibility of adsorption can also be ascertained, as only components that are retained after rinsing are analysed.

The techniques used in this work include both synchrotron XPS and conventional XPS. Synchrotron XPS offers greater potential for the acquisition of high quality adsorbed IL spectra than conventional XPS, allowing the dissection of complex photoemission peak envelopes [40] and thus providing more information on IL binding and structure. The IL studied is 1-hexyl-3-methyl-imidazolium bis(trifluoromethanesulfonyl) imide: HMIM NTf_2 (following on from earlier work on ultrathin HMIM NTf_2 precursor films on mica [41]). XPS analysis is complemented by spectroscopic ellipsometry studies of the adsorbed film. The data indicate that HMIM NTf_2 adsorbs irreversibly from ethanol, and forms (at least) a bilayer on the gold surface, with patchy coverage. The adsorbed layer is seen to be influenced by the degree of oxidation of the sputtered gold, and indications are seen of direct chemical interaction between the IL anion and the substrate.

EXPERIMENTAL METHODS

Materials: HMIM NTf_2 (99%) was purchased from Iolitec, Germany. Ethanol (100% undenatured, 99.5% v/v, AR), acetone (AR), H_2SO_4 (98%, AR) and H_2O_2 (30 %, AR) were purchased from Chem Supply, Australia. Milli-Q water of resistivity 18.2 MΩ·cm, total organic carbon less than 4 μg/l, and interfacial tension 72.4 ± 0.1 mN/m at 22 °C was produced by a Milli-Q™ Advantage A10 water purification system.

The gold substrates for the IL adsorption studies were fabricated using Physical Vapor Deposition (PVD). A 5 (± 2) nm layer of chromium (adhesion promoter) was sputtered onto a silicon wafer (p-type, <100>, Si-Mat Silicon Materials, Germany), followed by 100 (± 8) nm of gold. Prior to use, a 3 inch silicon wafer was cut to 12 × 12 mm pieces, sonicated in acetone (15 minutes), rinsed with copious amount of ethanol, sonicated in ethanol (15 minutes), rinsed with Milli-Q water and then dried with a nitrogen gun. The dried silicon wafers were then further cleaned by dipping in freshly prepared Piranha solution (H_2SO_4: 30% H_2O_2; 3:1 volume ratio) for 30 minutes, followed by rinsing with copious amount of Milli-Q water until neutral pH. The wafers were again dried with a nitrogen gun and moved to the sputter coater (TF 500, HHV Ltd., UK) chamber, and placed under vacuum. Prior to metal sputtering, a final silicon wafer cleaning step was carried out using an O_2 followed by an Ar plasma for 1 and 5 minutes, respectively. After the plasma cleaning, once the pressure in the chamber reached 7×10^{-7} mbar, sputtering in an argon environment commenced, using a DC magnetron source operating at 100 W. To ensure a homogenous film thickness, the substrate holder was rotated continuously at 15 RPM during sputtering. The target to substrate distance was 10 cm. Parameters used for chromium (99.99%) sputtering were as follows: frequency (50 kHz), and pulse widths of 8 μs at the 12 sccm Ar (and pressure $1.12\cdot10^{-2}$ mbar). In order to minimise any oxidation of the sputtered chromium layer, the sputtering of gold (99.99%) started immediately after the chromium deposition. Parameters

used for gold and silver sputtering were as follow: frequency 50 kHz, pulse width of 8 μs at 12 sccm Ar.

Substrates were cleaned in ethanol and isopropanol prior to immersion in 0.1 wt. % HMIM NTf_2 in ethanol solution for 12 hours. Treated samples were then rinsed in ethanol, dried in a stream of nitrogen gas, and then examined by XPS or ellipsometry.

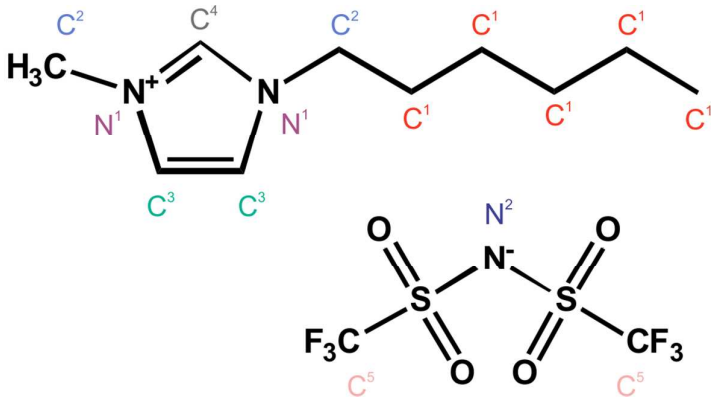

Figure 1. Chemical structure of HMIM NTf_2 (1-hexyl-3-methyl-imidazolium bis(trifluoromethanesulfonyl) imide. Numbered elements indicate different chemical environments.

Atomic Force Microscopy: AFM experiments were conducted inside a clean room (Class 1000). The AFM (Multimode 8 with a Nanoscope V controller, Bruker, USA) was mounted on an active antivibration table (Vision IsoStation, Newport). A vertical engagement scanner "E" (maximum scan range 10 μm in the in-plane x and y directions, and a nominal 2.5 μm in the normal to the surface z direction) was used. Rectangular cantilevers (NSG10, NT-MDT, Russia) with resonance frequencies between 140 and 390 kHz, and spring constants between 3.1 and 37. 6 N/m (single crystal silicon tip of tetrahedral shape and typical curvature radius

6-10 nm) were used for imaging of 1 × 1 μm^2 areas of the sputtered films. The images were acquired for multiple positions using tapping mode in air. The collected images were processed and analyzed using the WSxM 4.0 SPMAGE 09 Edition (Nanotec, Spain) [42] and NanoScope Analysis v1.5 (Bruker, USA) software packages.

Spectroscopic Ellipsometry: Spectroscopic ellipsometry is sensitive to sub-nanometre adsorbed layers,[43] and is thus ideal for studying small molecule adsorption to solid surfaces. Thickness measurements of the IL adsorbed on to the gold surfaces were performed using a vertical variable angle spectroscopic ellipsometer V-VASE (J. A. Woollam, USA). Before measurements, the ellipsometer was calibrated using a standardized SiO_2 wafer. Three samples of Au were examined in order to determine the properties of the substrate used. Three scans per single sample were taken, changing the spot on the sample on each occasion that it was scanned. In order to minimize errors, ellipsometric measurements were carried out for the same samples after IL adsorption. Measurements of the ellipsometric parameters (Ψ and Δ, the amplitude ratio and phase difference, respectively, of reflected p (r_p) and s (r_s) polarized light) were collected over the wavelength range of 400-1000 nm at an angle of incidence of 75°. Data analysis was performed using the WVASE32 software (JA Woollam, USA), with the adsorbed layer modeled as a Cauchy medium. The optical constants for the two metals were determined for bare substrates prior to analysis (for three incident angles – 65, 70, and 75 degrees – and for the full wavelength range of the ellipsometer – 250 nm to 1100 nm), to ensure that the fitting procedure for the IL-exposed metal was as accurate as possible.

Conventional XPS: The conventional XPS measurements were recorded with an AXIS Ultra spectrometer (Kratos, UK) using a monochromatic Al Kα source (hv = 1486.6 eV) operating at 15 kV and 10 mA. The pressure during analysis was 2 x 10^{-9} Torr. The spot size of analysis

was approximately 300 μm × 700 μm. The XPS data was processed using the CasaXPS program (version 2.3). Survey spectra were collected over a range of 0-1120 eV binding energy with a pass energy of 160 eV and 0.5 eV step size. High resolution spectra were collected with a pass energy of 20 eV for N 1s (0.1 eV step size) and for S 2p (0.05 eV step size). All binding energies were corrected using the Au $4f_{7/2}$ peak at 84.0 eV to compensate for surface charging effects. Each spectrum was acquired on a fresh spot of the substrates, and each spectrum (multiple scans) took no longer than 30 minutes to acquire. No evidence of sample beam damage was observed in the acquired spectra, as expected given the use of monochromatic X-rays and low exposure times (degradation has been observed with vapor deposited ILs on solid surfaces, but was only seen with a a lab-based X-ray source for long exposure times and the use of non-monochromatic X-rays [44]).

Synchrotron XPS: Synchrotron XPS (SXPS) was conducted using the Soft X-ray Spectroscopy beamline (14ID) at the Australian Synchrotron [45]. The insertion device for beamline 14ID is an elliptically polarized undulator providing a flux (at 400 eV) of between 5 × 10^{11} and 3 × 10^{12} Photons /s/ 200 mA at the sample, with a nominal beam area of 0.6 × 0.6 mm normal to the beam. The photon energy range of the beamline is 90 - 2600 eV with a resolution (E/ΔE) between 5000 and 10,000. The soft X-ray end-station has been described previously [14] and is equipped with a SPECS 150MCD photoemission energy analyzer. The analysis chamber vacuum was 2 x 10^{-10} Torr or better during spectral acquisition. High resolution spectra were collected using a pass energy of 10 eV and an energy step of 0.05 eV. The position of the Au $4f_{7/2}$ peak at 84.0 eV was used as the internal binding energy reference for all high resolution spectra.

The high resolution spectra for each element were collected with the same depth sensitivity (while avoiding overlapping Auger peaks). In each case, the spectra were collected using a

photon energy approximately 200 eV above the line of interest. A 200 eV electron kinetic energy yields an inelastic mean free path (IMFP) of approximately 0.9 nm for many organic compounds, based on the equations of Tanuma, Powell, and Penn [46], and calculated by the QUASES-IMFP-TPP2M program [47]. This IMFP yields an information depth (ID_{90}) of approximately 2.1 nm (depth from which 90% of the signal is detected), based on the simple expression for ID without inclusion of elastic scattering interactions [48], and with the detector normal to the analysed surface. The high resolution synchrotron XPS spectra were fitted using the CasaXPS program (version 2.3). The peak fitting function was a combination of 50 % Gaussian and 50 % Lorentzian (GL(50)), used to simulate a Voigt profile. The S 2*p* region fit was subject to a number of constraints: the S 2*p* peak of sulfur is a spin orbit split doublet (3/2,1/2), with an energy splitting of 1.19 eV, an intensity ratio of 2:1, and equal linewidth for each component of a doublet. A Shirley background was used in all spectral processing [49].

To minimize any potential damage of the adsorbed IL layer, samples were only exposed to the X-ray beam during analysis. Fresh spots of the sample were used for each spectrum recorded. Signal levels were sufficient to allow spectral acquisition within a few minutes. Within this time, two scans of each region were acquired for each spectrum. Only spectra for which there was no alteration in peak profile between the first and second scans were used for processing. Prolonged exposure in the X-ray beam was observed to alter the acquired spectra; details of this process, and its use to investigate X-ray induced desorption of IL is detailed in the Results and Discussion section below.

RESULTS AND DISCUSSION

Characterization of Gold films: As these experiments were performed on sputter-coated gold films rather than single crystal gold surfaces traditionally used in UHV surface chemistry studies, efforts were made to fully characterise the substrates prior to use in the adsorption

studies. The thickness and roughness of the deposited layers was assessed using tapping mode AFM. AFM height images (1 × 1 μm^2) as well as the cross-section of the height profiles of the gold film are presented in Figure 2. The root mean square (RMS) roughness of the gold film was 1.48 nm with a peak-to-valley (PTV) height of 11.47 nm over a 1 μm^2 area. The AFM height images in Figure 2, together with the roughness data, show that the gold substrate is relatively smooth: the image surface area is approximately 2% greater than the image projected surface area for a planar surface.

In addition, even though there is roughness of dimensions greater than the anticipated thickness of a molecular layer of adsorbate, the collection of the emitted photoelectrons at an angle normal to the surface (which was the case for both conventional and synchrotron XPS) ensures that the roughness will not overly affect the information/analysis depth of the XPS measurements.

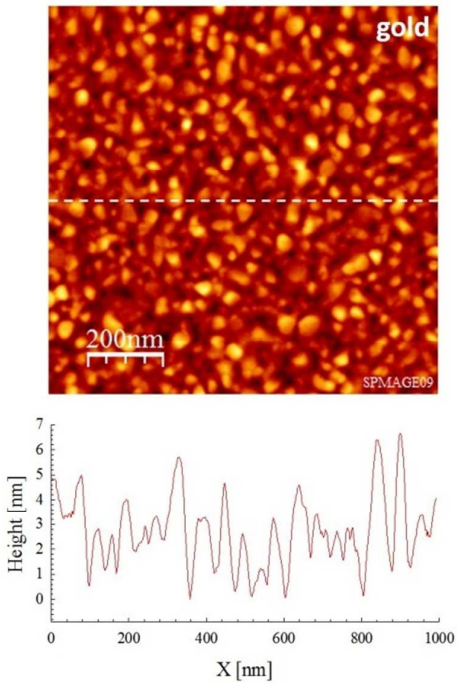

Figure 2. AFM 1 × 1 μm^2 height images (top) and a cross-section height profile along the dashed line (bottom) for a sputtered gold substrate.

To ensure that the spectral and ellipsometric signals detected on the gold substrates are due to adsorption of IL, a number of conventional XPS survey scans of gold substrates exposed to varying solution treatments (without the presence of IL) were acquired to determine the nature of the pre-adsorption gold substrate. These XPS spectra are given in Figure 3. Surveys were acquired for freshly sputtered gold, for gold exposed to an ethanol/isopropanol cleaning step, for gold cleaned using Piranha solution for 30 min, and for gold cleaned with ethanol/isopropanol and then exposed to ethanol for 12 hours (without IL present).

All four spectra look remarkably similar. The major peaks are due to gold, and there are additional small peaks due to carbon and oxygen. The surface atomic concentration of the carbon on the gold surfaces is between 20-26%. This carbon is termed adventitious carbon [50], and is present as a result of exposure of the clean (high surface energy) gold substrates to air between cleaning and placement in the XPS instrument. This material will not interfere with the adsorption of ionic liquid as the clean gold is placed into the IL/ethanol solution immediately after cleaning.

One feature that does change between the spectra is the signal from the O 1*s* peak at approx. 530 eV. For freshly sputtered gold, solvent cleaned gold, and Piranha cleaned gold, the oxygen makes up less than 1% of the surface atoms detected (although it is slightly higher on Piranha cleaned gold, which agrees with previous research that shows that Piranha cleaning can cause oxidation of gold substrates, and thus change the surface properties [51]). Exposure to ethanol for 12 hours causes some additional oxidation of the gold substrate, with 3% of the surface atoms detected being oxygen. No other elements were detected on the surface of the sputtered gold substrates.

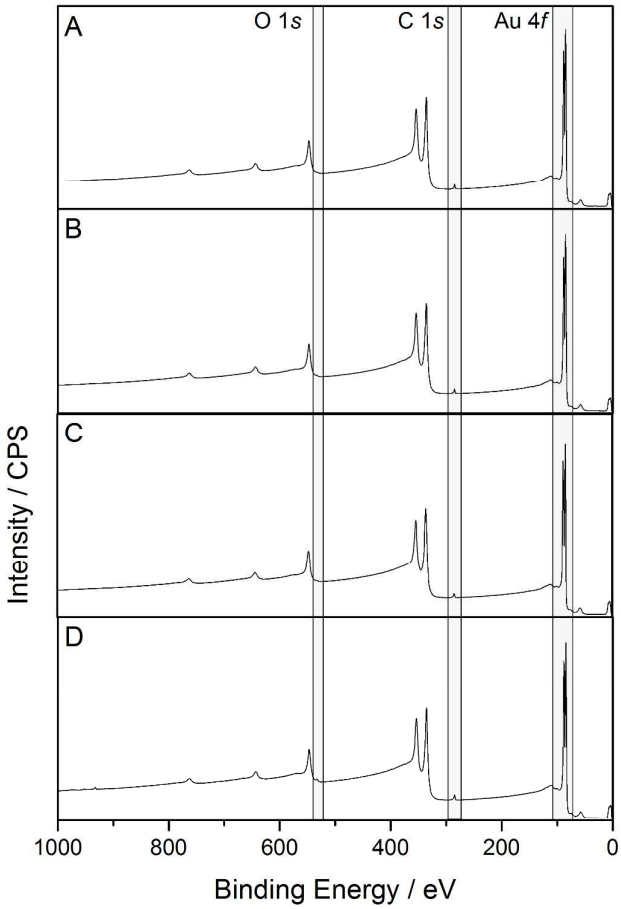

Figure 3. Conventional XPS survey scans of: A – freshly sputtered gold; B – solvent washed gold; C – Piranha cleaned gold; and D – gold substrate exposed to ethanol for 12 hours. Shaded regions provide emphasis for the three photoemission peaks used to determine atomic surface concentrations.

Adsorption of HMIM NTf_2 on Gold: Ellipsometry: The adsorption of HMIM NTf_2 on gold was first interrogated using spectroscopic ellipsometry. The ellipsometric parameters of Ψ and Δ were acquired for three different incident angles, and for the wavelength range from 250 nm to 1100 nm, thus providing sufficient data to allow unambiguous determination of the IL layer thickness on the substrate.

Data for the two parameters as a function of incident light wavelength are given in Figure 4. The model fit for determination of thickness is also provided: the raw data and fitted ellipsometric response are in very good agreement. The thickness value of the adsorbed film of IL was determined to be 0.15 ± 0.02 nm (determined as the average of nine measurements: three samples of the gold substrate; and three measurement spots were interrogated for each sample). The thickness value is smaller than that expected for an ion pair [52], and does not correlate with the length of a cation, as determined either geometrically (1.3 nm) or from AFM images of cation layers on substrates (between 0.4 nm to 0.8 nm for shorter chain imidazolium/ NTf_2 ionic liquids) [53]. However, ellipsometry is a measurement method that determines an average thickness over a large area, and is therefore subject to complications should an adsorbed layer not be continuous over a substrate. It is likely that for HMIM NTf_2 on gold, the adsorbed layer of IL is patchy.

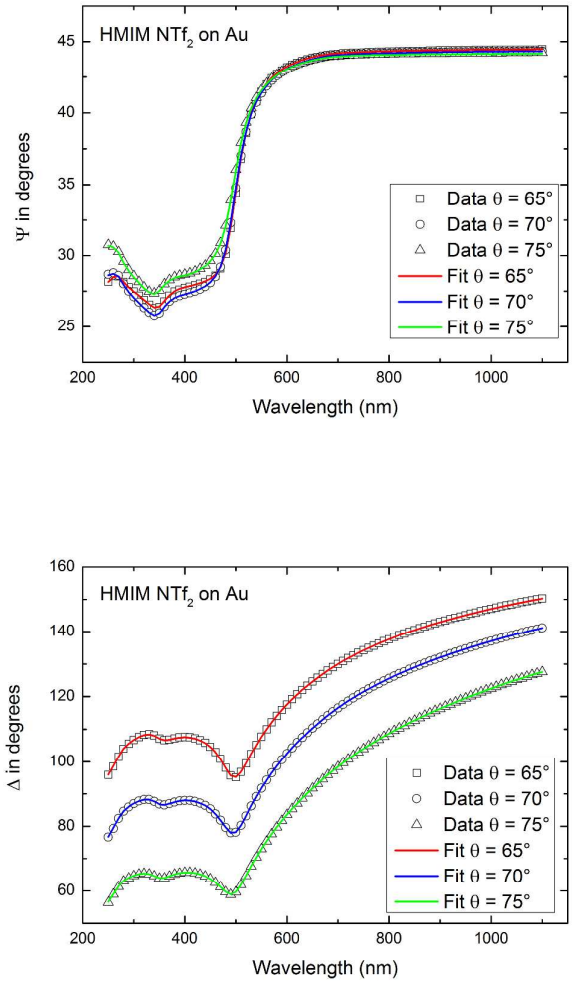

Figure 4. Variation of Ψ (top) and Δ (bottom) (ellipsometric parameters, the amplitude ratio and phase difference, respectively, of reflected p (r_p) and s (r_s) polarized light) with incident wavelength for gold exposed to HMIM NTf_2 for 12 hours from a solution of 0.1 wt. % in ethanol. Also included are fitted values of Ψ and Δ for the adsorbed layer of HMIM NTf_2 on the metal.

Adsorption of HMIM NTf_2 on Gold: Conventional XPS: Conventional XPS spectra (survey scan and high resolution scans) were recorded for the gold substrate exposed to a 0.1 wt. % solution on HMIM NTf_2 in ethanol. These spectra are given in Figure 5. The survey scan is shown in the top of Figure 5, and the photoemission peaks observed are those to be expected for an adsorbed layer of HMIM NTf_2, both cation and anion. F 1*s*, O 1*s*, N 1*s*, C 1*s*, and S 2*p* peaks are all observed. Quantification of the surface atomic concentrations yields the following percentages: C – 49.3 %; F – 22.7 %; O – 12.1 %; N – 10.6 %; S – 5.2 %. The lowest kinetic energy of the photoelectrons detected (from the F 1*s* orbital), result in an information depth (ID_{90}) of at least 3 nm. This indicates that the measurement will sample the complete adsorbed layer (if we assume that it is no thicker than an ion pair, which is a sensible assumption based on the ellipsometry measurement), and thus provide accurate stoichiometry of the layer.

The number of atoms for an ion pair of HMIM NTf_2 is: C – 12; F – 6; O – 4; N – 3; S – 2. This translates to the following approximate stoichiometric percentages: C – 44.5 %; F – 22.2 %; O – 14.8 %; N – 11.1 %; S – 7.4 %. The close match between the stoichiometric percentage of an ion pair of HMIM NTf_2 and the detected surface atomic percentages of the adsorbed HMIM NTf_2 film indicates two things: (i) there is no significant hydrocarbon contamination in the adsorbed layer; (ii) the anion and cation are present on gold in relatively equal amounts.

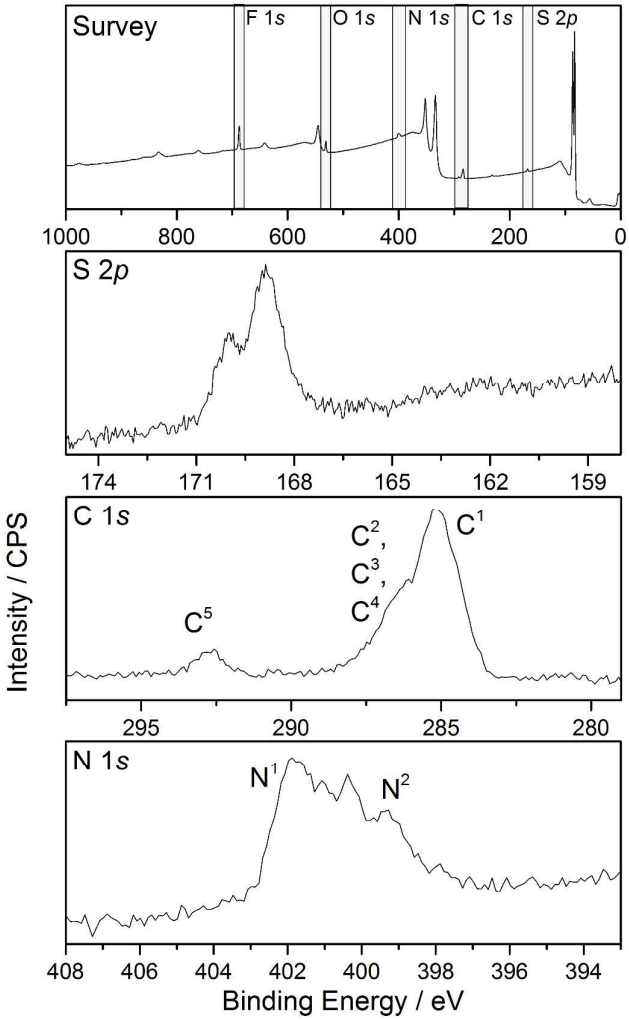

Figure 5. Conventional XPS spectra (survey and high resolution scans) of HMIM NTf_2 adsorbed layer on gold (adsorbed from 0.1 wt. % solution in ethanol).

The high resolution spectra of the S 2*p*, C 1*s*, and N 1*s* regions are given in the panels below the survey scan. The spectra reveal a number of important pieces of information. In the S 2*p* spectrum of bulk liquid HMIM NTf_2 there a single peak doublet at approximately 169 eV [54] due to the NTf_2 anion. This peak is also present in the spectrum for the adsorbed layer, indicating that there is an anion component in the adsorbed layer.

The C 1*s* spectrum contains 3 distinct peak components that indicate the presence of both cation and anion. The peak component at approx. 292.5 eV is assigned to the C-F carbons in the anion (C^5 in Figure 1)[32, 54]. With reference to Figure 1, there are four distinct chemical environments for carbon atoms in the HMIM cation: aliphatic chain (C^1, peak at 285.0 eV), aliphatic C-N with the carbon bonded to only one nitrogen (C^2), aromatic C-N with the carbon only bonded to one nitrogen (C^3 in the imidazolium ring), and aromatic C-N with the carbon bonded to two nitrogens (C^4 in the imidazolium ring). The aliphatic C (C^1) and the C-F components (C^5) can be identified clearly in the spectrum. However, the energies of the three C-N carbon environments are so close (between 286 eV and 287 eV) that they form a single peak shoulder comprised of 3 unresolved overlapping components. No spectral deconvolution was attempted on the C 1*s* region, as numerous assumptions would be required (e.g. peak positions *and* peak widths) that cannot be simply justified.

Nitrogen is present in both the anion and cation, and nitrogen is the locus for the equal and opposite charge on the two IL components. Bulk imidazolium NTf_2 ionic liquids have two N 1*s* peak components at approx. 402 eV (cation – N^1) and 399 eV (anion – N^2) [32, 41, 54]. If both anion and cation are present in the adsorbed layer then we would expect that we would observe two distinct components in the adsorbed layer spectrum. Upon inspection of the N 1*s* spectrum in Figure 5, two peaks can be discerned in the profile at those energies, and are assigned to the cation and anion in the adsorbed layer. However, the profile appears to have two additional components – one between the two assigned peaks, and one to lower binding energy than the anion peak. These additional components indicate some heterogeneity in the chemical environment of the anion and cation.

Adsorption of HMIM NTf_2 on Gold: Synchrotron XPS: High resolution synchrotron XPS spectra of HMIM NTf_2 adsorbed onto sputtered gold are presented in Figure 6. High resolution scans were acquired for the different elements using a photon energy that ensures collection of similar kinetic energy photoelectrons (and thus depth of sampling). The spectra in Figure 6 are of much higher signal-to-noise than the conventional XPS spectra presented in Figure 5. As with the conventional survey scan in Figure 5, the observation of a peak due to photoemission from the F 1*s* orbital confirms unambiguously the presence of the NTf_2 anion adsorbed at the surface of gold. The C 1*s* spectrum has the same features as the conventional high resolution C 1*s* spectrum, with the three clearly distinct chemical environments that indicate the presence of the anion and cation at the surface

The synchrotron XPS high resolution O 1*s* spectrum provides additional details about the ionic liquid and the substrate. Oxygen is present in the NTf_2 anion in a single chemical environment. However, the O 1*s* region contains a peak that can be deconvoluted into two components, one at 532.4 eV, and the other at 530.8 eV. The higher binding energy component is assigned to the oxygen in the anion [32, 54], whilst the lower binding energy component is attributed to residual oxidation of the gold substrate [55, 56], whose presence on gold is almost ubiquitous after substrate cleaning [51]. This is in agreement with the substrate XPS characterisation shown in Figure 3.

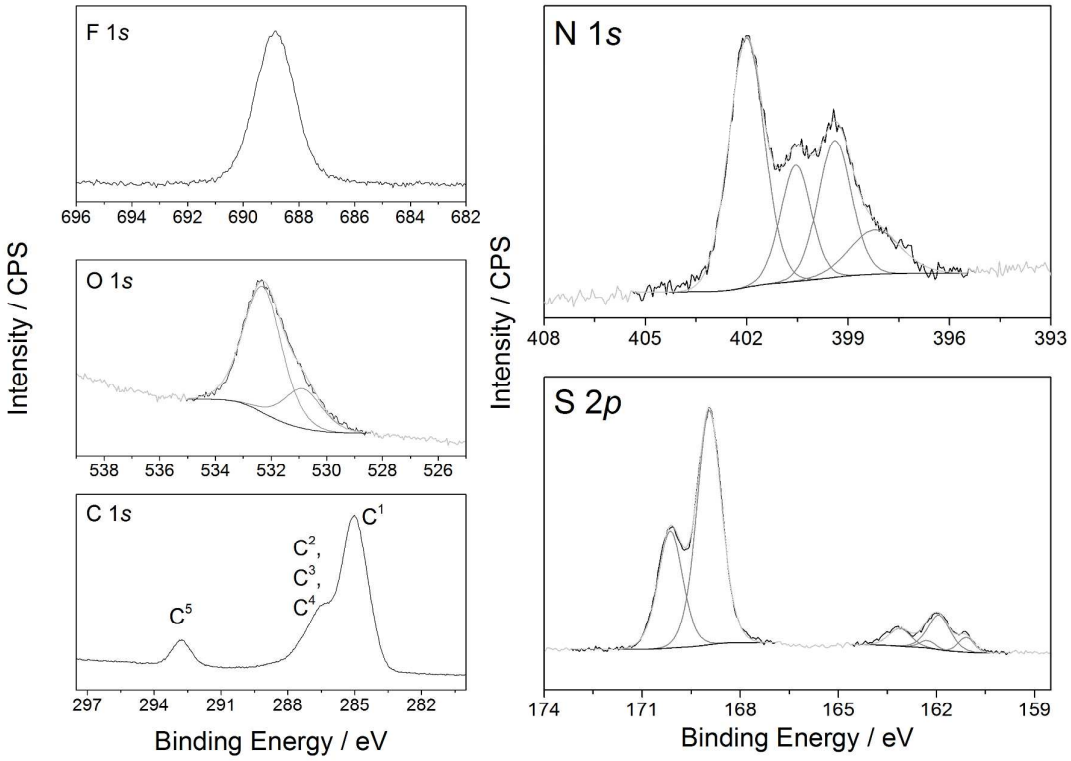

Figure 6. XPS high resolution scans for HMIM NTf_2 on gold: F 1*s* (hν = 900 eV), O 1*s* (hν = 700 eV), C 1*s* (hν = 440 eV), N 1*s* (hν = 600 eV) and S 2*p* (hν = 340 eV). Spectra plotted for O 1*s*, N 1*s*, and S 2*p* include peak deconvolutions.

The N 1*s* spectrum is shown in the upper right-hand panel in Figure 6. The good signal to noise allows for peak deconvolution, and this confirms that there are four components to the N 1*s* peak envelope (in agreement with the N 1*s* spectrum in Figure 5) – see Table 1 for details of the peak components. The peaks at 402.0 eV and 399.5 eV are assigned to the cation and anion, respectively [32, 41]. Their positions are the same as the bulk IL. The two other peaks, falling on the lower binding energy side of both major cation and anion peaks, are assigned to cation and anion directly interacting with the gold. This assignment is made based on the work of Cremer et al. [34] who studied imidazolium NTf_2 ILs vapor deposited on

gold, and detected distinct peak position differences for the anion and cation N peaks, dependent on whether the species were in direct contact with the metal, or were part of a physisorbed multilayer. In their work, a gradual progression from low signal (low binding energy) bound N to high signal (high binding energy) multilayer N was observed. In this case, we detect both the surface-bound and the liquid-like anion and cation, giving an indication that there may be bilayer or multilayer adsorption of the ionic liquid from ethanol.

Given that the N 1*s* region contains peaks due to both species, it is useful to compare the relative amounts of anion and cation nitrogen. The deconvolution into both bound and liquid-like IL provides us with two stoichiometric comparisons. Taking the liquid-like components first, it can be seen from Table 1 that the area ratio of cation N to anion N is approximately 2:1; stoichiometrically correct for ion pairs. For the surface bound components, this ratio is also 2:1, which indicates either ion pair adsorption, or that equal amounts of cation and anion are directly interacting with gold. The conclusions from analyzing the N 1*s* component ratios agree with the conventional XPS survey scan atomic surface concentrations (i.e. anion and cation present in equal amounts in the adsorbed layer).

Figure 6 also contains the spectrum and peak deconvolution of the S 2*p* signal for the adsorbed IL layer on gold (lower panel, right-hand side) – see Table 1 for the peak components. The synchrotron XPS spectrum reveals the presence of additional S 2*p* peaks at lower binding energy. These peaks were too low in relative intensity compared to the liquid-like S 2*p* peak to be detected with conventional XPS, due to the much poorer signal-to-noise. The fitting of the bulk liquid-like anion S produces the expected doublet at approximately 169 eV. The fitting also reveals that there are in fact an additional two S 2*p* doublets at much lower binding energy (between 161 and 162 eV – see Table 1). These doublets are in a

binding energy region reflecting strong chemical interaction with the underlying metal [40, 57-60].

Interaction of the NTf_2 anion with gold has been observed in studies on the formation of gold nanostructures [11], thus some degree of chemical interaction might be expected. In addition, in electrochemical experiments [61] and vapor deposition experiments [37, 38] with lithium and copper metal with ionic liquids containing the NTf_2 (and related) anion, there is evidence for direct anion-metal interactions and reactions (including the detection of lower binding energy S 2*p* doublets on copper [38]). Furthermore, NMR studies of the interaction of the NTf_2 anion on Mg metal has shown indications of reactions and NTf_2 anion breakdown at the metal interface [7]. It is possible that the chemically bound S signal observed here in Figure 6 is due to a small amount of NTf_2 anion that has reacted with/broken down at the gold interface during the adsorption process, allowing the classic Au-S bond to be formed. Whether this interaction is occurring due to some electrochemical mechanism or some aspect of ionic liquid decomposition in the solvent cannot be determined from this current work. However, based on the relative intensity of the intact anion sulfur and the chemically bound sulfur, there is only a small proportion of anions that have undergone this transformation on the gold substrate.

Table 1. S 2*p* and N 1*s* peak deconvolution, binding energies, abundances, widths, and assignments for HMIM NTf_2 adsorbed on Au.

Element	Binding Energy (eV)	Abundance (%)[a]	FWHM (eV)	Assignment
S $2p_{3/2}$	161.1	3	0.5	Chemisorbed S/metal sulfide [57-60]
	162.0	12	0.8	Chemisorbed S/metal sulfide [57-60]
	169.0	85	0.9	Sulfur oxy species sulfate [54]
N 1*s*	398.2	10	1.7	Interacting anion [34]
	399.5	25	1.2	Anion N [32, 54]
	400.5	19	1.1	Interacting cation [34]
	402.0	46	1.2	Cation N [32, 54]

[a] abundance refers to the relative abundance (in percent) of the different components in the peak deconvolution

HMIM NTf_2 on Au – Adsorbed Layer Structure: The data presented allows a picture of the adsorbed layer structure to be formulated. Both anion and cation are present in the adsorbed layer, in stoichiometric amounts. There is evidence of at least bilayer features in the N 1*s* XPS spectra (conventional and synchrotron), and there is an indication from the synchrotron XPS of a small amount of direct S binding to the gold substrate (signal too weak to be seen in conventional XPS). The ellipsometry data indicate that the adsorbed layer is patchy (due to the measurement of a thickness smaller than the ion-pair diameter).

The explanation for patchy coverage is most likely one of three possibilities: (i) simple low affinity of the ionic liquid components for the gold substrates; (ii) inhibition of adsorption due to the presence of adventitious hydrocarbon contamination; and (iii) differing affinity of the ionic liquid components for oxidized gold (spectra shown in Figures 3 and 6 indicate the presence of some metal oxide at the surface of the gold). In terms of the first possibility, the XPS spectra exhibit clear indications of interaction between the cation and the anion with the

two metal surfaces. In the case of the cation, this comes from the N 1*s* spectra (presence of the lower binding energy cation N 1*s* peak). In the case of the anion, there is the N 1*s* spectra (presence of the lower binding energy anion N 1*s* peak) *and* the S 2*p* spectra (doublets at an energy that indicates direct chemical interaction between the anion, or some component of the anion) and the gold substrate. These observations would suggest that the ionic liquid has a high affinity for gold. The second possibility (inhibition due to presence of surface contaminants) is undermined by the close match in expected stoichiometry from the conventional XPS survey scan with that of an ion pair. Excessive hydrocarbon contamination would result in a strong bias toward carbon, which is not observed.

The third possibility (differing affinity for gold relative to gold oxide) was tested by adsorbing HMIM NTf_2 onto gold substrates that were Piranha cleaned as opposed to cleaning with solvent washing. Piranha-cleaned gold is known to be altered in terms of the surface chemistry, with gold oxide formed, changes in hydrophobicity, and changes in surface charge [51]. If the metal oxide presents a less attractive interface for adsorption compared to the un-oxidised metal, Piranha-cleaned gold substrates treated with IL solution would give rise to lower signals than solvent-cleaned gold. An XPS spectrum was recorded of the S 2*p* region for HMIM NTf_2 adsorbed on Piranha-cleaned gold; this spectrum is plotted in Figure 7, along with the spectrum of the S 2*p* region of HMIM NTf_2 adsorbed on solvent cleaned gold (replotted from Figure 6). Both spectra were recorded with identical scan and sample conditions, and are plotted on the same X-Y scale (although offset vertically for clarity). It can be seen clearly that there is a signal decrease for the S 2*p* spectrum of HMIM NTf_2 on the Piranha-cleaned gold substrate, relative to the solvent cleaned substrate. The overall signal intensity of the S region is significantly lower for the Piranha cleaned gold sample, and the relative ratio of bound S to 'liquid-like' S is also different (solvent 15:85, Piranha 10:90).

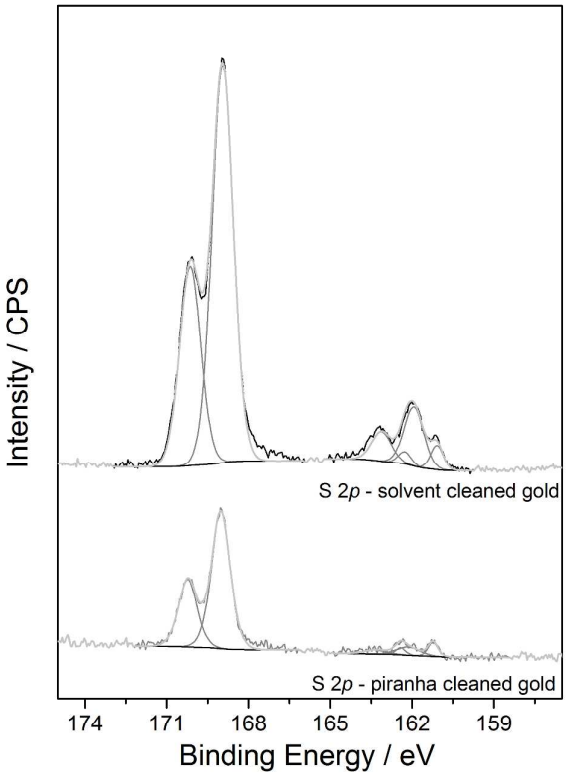

Figure 7. XPS high resolution scans for HMIM NTf_2 on gold: S 2*p*. Scan on the top panel is that presented in the Figure 6, with a solvent cleaned gold substrate. Scan on the lower panel is that recorded with Piranha cleaned gold. Identical adsorption and spectral acquisition conditions were used, with the same scan parameters.

A preference for non-oxidised metal for adsorption can thus explain the partial coating of the solvent cleaned gold substrate. IL adsorbed on oxidized regions of the metal surface may well be more easily removed during the ethanol rinse performed prior to all experiments. Although not definitive, the hypothesis that IL-metal interactions are stronger with un-oxidised metal surfaces is supported by the available spectral evidence, and this provides a viable explanation to the observation of patchy IL coverage on gold.

Further information concerning the structure of the adsorbed layer can be obtained by making use of the brightness of the synchrotron X-ray beam. The N 1*s* region of the XPS spectra of HMIM NTf_2 on gold was investigated in more detail using prolonged exposure to the X-ray beam. Instead of blocking the incident X-ray beam between spectra and recording scans on fresh spots for each measurement, two spectra were recorded on the same spot (with identical scan parameters) with a few minutes of additional exposure in between scans. Two such spectra are given in Figure 8. Peak deconvolutions, based on the peak positions and peak widths determined from the fitting shown in Figure 6, are also shown. It can be seen that there is a distinct alteration in the relative signals of the surface interacting and the non-interacting components of the IL adsorbed layer. The second spectrum has a much higher contribution from the bound components (both anion and cation), with the intensity of the non-interacting components both reduced. This is consistent with the X-ray beam essentially desorbing the cation and anion in the uppermost 'liquid-like' component of the adsorbed layer, with the bound components now more visible to the probe X-ray beam. It also indicates that there is a mixture of anion and cation in the layer immediately adjacent to the gold surface, and a mixture of anion and cation in the layer above. There is no preferential adsorption of anion over cation (or vice versa) on the gold substrate.

It should be noted here that a comparison of the N 1*s* spectra in Figures 5 and 6 supports the conclusion from the prolonged exposure data. The spectrum in Figure 6 (synchrotron – ID_{90} of 2.1 nm) has greater intensity in the 'liquid-like' components relative to the surface bound components, when compared to the spectrum in Figure 5 (conventional – ID_{90} of greater than 3 nm).

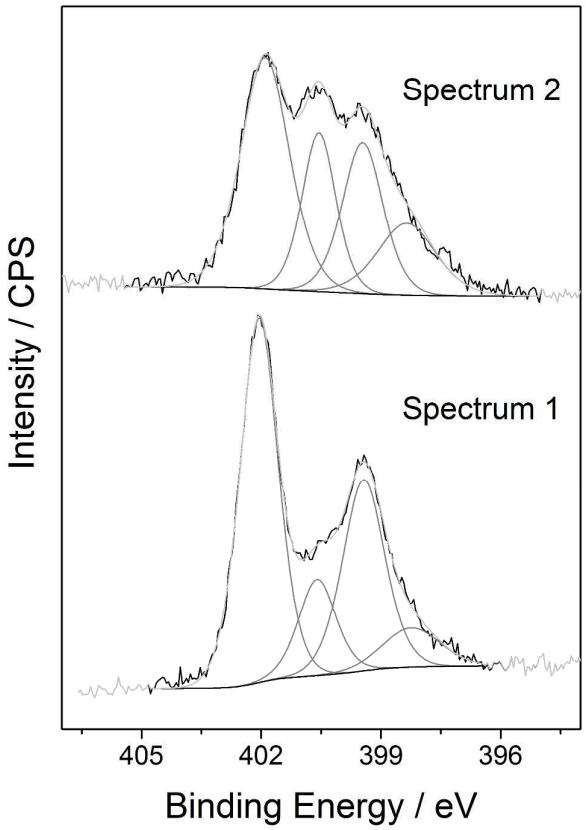

Figure 8. XPS high resolution scans of the N1*s* region: sequentially recorded spectra on the same spot of a HMIM NTf_2/Au sample; the two traces are offset vertically for clarity.

The combined spectral evidence allows us to propose the following structure for HMIM NTf_2 adsorbed on gold: (i) patchy coverage; (ii) equal amounts of cation and anion in layer immediately adjacent to the surface; (iii) equal amount of cation and anion in the layer above; (iv) areas of gold oxide exposed. The structure is shown in Figure 9. The model bears some similarities to that suggested for physical vapour deposited MMIM NTf_2 and OMIM NTf_2 on gold at high coverage [34]. However, it is difficult to draw comparisons due to the differences between the substrate (single crystal gold versus sputter-coated gold), the ionic liquid (HMIM NTf_2 used here), and the different methods of adsorption. In addition, there are distinct

differences in the spectral evidence that led to this proposed structure (partial coverage even for bilayer adsorption; presence of chemically interacting anion in small amounts). These features point toward the importance of studying ionic liquid interactions with 'real' surfaces rather than pristine single crystal surfaces, which may not be representative of many applications (electrochemistry, lubrication, etc.).

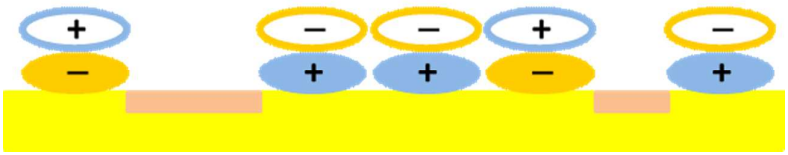

Figure 9. Schematic diagram of the adsorbed layer of HMIM NTf_2 on gold. A partial coating of interacting 'bound' anion (filled orange) and 'bound' cation (filled blue) exists nearest to the surface, on top of which is non-interacting cation (empty blue, atop interacting anion) and non-interacting anion (empty orange, atop interacting cation). Bare regions of the substrate represent areas of oxidized gold, and are indicated by a darker colour.

CONCLUSION

The adsorption of HMIM NTf_2 onto sputter-coated gold from ethanol solutions has been studied with conventional XPS, synchrotron XPS, and spectroscopic ellipsometry. The combination of layer thickness data and spectral observations has enabled a detailed picture to be developed for the structure and composition of the adsorbed IL layer on gold. A patchy layer of adsorbed IL, consisting of interacting IL components (with some evidence for chemically-bound IL components) and liquid-like IL on top of these regions is consistent

with the observations from the different techniques. The need for unoxidised metal for significant adsorption is postulated, which is consistent with the sample preparation methods. The nature of the adsorbed layer on the metal substrate will have an influence on how this particular IL is used in applications such as lubrication and lubrication additives.

ACKNOWLEDGMENT

This work was performed in part on the soft X-ray beamline at the Australian Synchrotron, Victoria, Australia. The authors warmly acknowledge Dr Bruce Cowie and Dr Anton Tadich, beamline scientists at the soft X-ray beamline, for their assistance in operating the X-ray photoelectron end-station. This work was performed in part at the South Australian node of the Australian National Fabrication Facility, a company established under the National Collaborative Research Infrastructure Strategy to provide nano and micro-fabrication facilities for Australia's researchers. The authors acknowledge the financial support from the Swiss National Science Foundation Sinergia scheme, grant no. 136191 *'Designing interactions across interfaces in ionic liquids'*. DAB acknowledges the financial support from the Australian Research Council (ARC: Future Fellowship FT100100393; Discovery Project DP110104179).

REFERENCES

1. F. Zhou, Y. M. Liang and W. M. Liu, *Chem. Soc. Rev.*, 2009, 38, 2590-2599.
2. A. E. Somers, S. M. Biddulph, P. C. Howlett, J. Sun, D. R. MacFarlane and M. Forsyth, *PCCP*, 2012, 14, 8224-8231.
3. J. Qu, D. G. Bansal, B. Yu, J. Y. Howe, H. Luo, S. Dai, H. Li, P. J. Blau, B. G. Bunting, G. Mordukhovich and D. J. Smolenski, *ACS Appl. Mater. Int.*, 2012, 4, 997-1002.
4. B. Yu, D. G. Bansal, J. Qu, X. Sun, H. Luo, S. Dai, P. J. Blau, B. G. Bunting, G. Mordukhovich and D. J. Smolenski, *Wear*, 2012, 289, 58-64.
5. B. Khemchandani, A. Somers, P. Howlett, A. K. Jaiswal, E. Sayanna and M. Forsyth, *Tribology International*, 2014, 77, 171-177.
6. A. E. Somers, B. Khemchandani, P. C. Howlett, J. Sun, D. R. Macfarlane and M. Forsyth, *ACS Appl. Mater. Int.*, 2013, 5, 11544-11553.

7. M. Forsyth, W. C. Neil, P. C. Howlett, D. R. MacFarlane, B. R. W. Hinton, N. Rocher, T. F. Kemp and M. E. Smith, *ACS Appl. Mater. Int.*, 2009, 1, 1045-1052.
8. J. Dupont and J. D. Scholten, *Chem. Soc. Rev.*, 2010, 39, 1780-1804.
9. C. Vollmer and C. Janiak, *Coord. Chem. Rev.*, 2011, 255, 2039-2057.
10. T. Uematsu, M. Baba, Y. Oshima, T. Tsuda, T. Torimoto and S. Kuwabata, *J. Am. Chem. Soc.*, 2014, 136, 13789-13797.
11. L. Ren, L. Meng, Q. Lu, Z. Fei and P. J. Dyson, *J. Colloid Interface Sci.*, 2008, 323, 260-266.
12. H. S. Schrekker, M. A. Gelesky, M. P. Stracke, C. M. L. Schrekker, G. Machado, S. R. Teixeira, J. C. Rubim and J. Dupont, *J. Colloid Interface Sci.*, 2007, 316, 189-195.
13. V. Lockett, M. Horne, R. Sedev, T. Rodopoulos and J. Ralston, *PCCP*, 2010, 12, 12499-12512.
14. V. Lockett, R. Sedev, J. Ralston, M. Horne and T. Rodopoulos, *J. Phys. Chem. C*, 2008, 112, 7486-7495.
15. M. V. Fedorov and A. A. Kornyshev, *Chem. Rev.*, 2014, 114, 2978-3036.
16. Y. W. Zhu, S. Murali, M. D. Stoller, K. J. Ganesh, W. W. Cai, P. J. Ferreira, A. Pirkle, R. M. Wallace, K. A. Cychosz, M. Thommes, D. Su, E. A. Stach and R. S. Ruoff, *Science*, 2011, 332, 1537-1541.
17. M. Mezger, H. Schröder, H. Reichert, S. Schramm, J. S. Okasinski, S. Schöder, V. Honkimäki, M. Deutsch, B. M. Ocko, J. Ralston, M. Rohwerder, M. Stratmann and H. Dosch, *Science*, 2008, 322, 424-428.
18. R. M. Espinosa-Marzal, A. Arcifa, A. Rossi and N. D. Spencer, *J. Phys. Chem. C*, 2014, 118, 6491-6503.
19. R. M. Espinosa-Marzal, A. Arcifa, A. Rossi and N. D. Spencer, *J. Phys. Chem. Lett.*, 2014, 5, 179-184.
20. F. Federici Canova, H. Matsubara, M. Mizukami, K. Kurihara and A. L. Shluger, *PCCP*, 2014, 16, 8247-8256.
21. K. Ueno, M. Kasuya, M. Watanabe, M. Mizukami and K. Kurihara, *PCCP*, 2010, 12, 4066-4071.
22. M. Paneru, C. Priest, R. Sedev and J. Ralston, *J. Am. Chem. Soc.*, 2010, 132, 8301-8308.
23. M. Paneru, C. Priest, R. Sedev and J. Ralston, *J. Phys. Chem. C*, 2010, 114, 8383-8388.
24. H. Li, M. Paneru, R. Sedev and J. Ralston, *Langmuir*, 2013, 29, 2631-2639.
25. R. S. Kuhnel, S. Obeidi, M. Lubke, A. Lex-Balducci and A. Balducci, *J. Appl. Electrochem.*, 2013, 43, 697-704.
26. K. Yao, W. Lu, X. Li, J. Wang and J. Yuan, *Chem. Commun.*, 2013, 49, 1398-1400.
27. J. C. Rubim, F. A. Trindade, M. A. Gelesky, R. F. Aroca and J. Dupont, *J. Phys. Chem. C*, 2008, 112, 19670-19675.
28. Y. X. Yuan, T. C. Niu, M. M. Xu, J. L. Yao and R. A. Gu, *Journal of Raman Spectroscopy*, 2010, 41, 516-523.
29. S. Baldelli, *J. Phys. Chem. Lett.*, 2013, 4, 244-252.
30. S. G. Harroun, T. J. Abraham, C. Prudhoe, Y. Zhang, P. J. Scammells, C. L. Brosseau, C. C. Pye and R. D. Singer, *PCCP*, 2013, 15, 19205-19212.
31. V. Lockett, R. Sedev, C. Bassell and J. Ralston, *PCCP*, 2008, 10, 1330-1335.
32. V. Lockett, R. Sedev, S. Harmer, J. Ralston, M. Horne and T. Rodopoulos, *PCCP*, 2010, 12, 13816-13827.
33. H. P. Steinrück, *PCCP*, 2012, 14, 5010-5029.
34. T. Cremer, M. Stark, A. Deyko, H. P. Steinrück and F. Maier, *Langmuir*, 2011, 27, 3662-3671.

35. A. Deyko, T. Cremer, F. Rietzler, S. Perkin, L. Crowhurst, T. Welton, H. P. Steinruck and F. Maier, *J. Phys. Chem. C*, 2013, 117, 5101-5111.
36. B. Uhl, T. Cremer, M. Roos, F. Maier, H. P. Steinruck and J. Behm, *PCCP*, 2013, 15, 17295-17302.
37. M. Olschewski, R. Gustus, M. Marschewski, O. Hofft and F. Endres, *PCCP*, 2014, 16, 25969-25977.
38. B. Uhl, F. Buchner, S. Gabler, M. Bozorgchenani and R. Jürgen Behm, *Chem. Commun.*, 2014, 50, 8601-8604.
39. S. Stolte, S. Steudte, O. Areitioaurtena, F. Pagano, J. Thöming, P. Stepnowski and A. Igartua, *Chemosphere*, 2012, 89, 1135-1141.
40. D. A. Beattie, I. M. Kempson, L.-J. Fan and W. M. Skinner, *Int. J. Miner. Process.*, 2009, 92, 162-168.
41. D. A. Beattie, R. M. Espinosa-Marzal, T. T. M. Ho, M. N. Popescu, J. Ralston, C. J. E. Richard, P. M. F. Sellapperumage and M. Krasowska, *J. Phys. Chem. C*, 2013, 117, 23676-23684.
42. I. Horcas, R. Fernandez, J. M. Gomez-Rodriguez, J. Colchero, J. Gomez-Herrero and A. M. Baro, *Rev. Sci. Instr.*, 2007, 78, 013705.
43. J. N. Hilfiker, N. Singh, T. Tiwald, D. Convey, S. M. Smith, J. H. Baker and H. G. Tompkins, *Thin Solid Films*, 2008, 516, 7979-7989.
44. A. Keppler, M. Himmerlich, T. Ikari, M. Marschewski, E. Pachomow, O. Hofft, W. Maus-Friedrichs, F. Endres and S. Krischok, *PCCP*, 2011, 13, 1174-1181.
45. B. C. C. Cowie, A. Tadich and L. Thomsen, 2010.
46. S. Tanuma, C. J. Powell and D. R. Penn, *Surf. Interface Anal.*, 1994, 21, 165-176.
47. S. Tougaard, 2010.
48. A. Jablonski and C. J. Powell, *J. Vac. Sci. Technol., A*, 2003, 21, 274-283.
49. D. A. Shirley, *Phys. Rev. B: Condens. Matter*, 1972, 5, 4709.
50. S. Evans, *Surf. Interface Anal.*, 1997, 25, 924-930.
51. R. F. Tabor, A. J. Morfa, F. Grieser, D. Y. C. Chan and R. R. Dagastine, *Langmuir*, 2011, 27, 6026-6030.
52. H. Li, M. Paneru, R. Sedev and J. Ralston, *Langmuir*, 2013, 29, 2631-2639.
53. Z. Wang and C. Priest, *Langmuir*, 2013, 29, 11344-11353.
54. E. F. Smith, F. J. M. Rutten, I. J. Villar-Garcia, D. Briggs and P. Licence, *Langmuir*, 2006, 22, 9386-9392.
55. Z. Zheng, M. Yang and B. Zhang, *J. Phys. Chem. C*, 2008, 112, 6597-6604.
56. B. Koslowski, H. G. Boyen, C. Wilderotter, G. Kastle, P. Ziemann, R. Wahrenberg and P. Oelhafen, *Surf. Sci.*, 2001, 475, 1-10.
57. C. Shen, M. Haryono, A. Grohmann, M. Buck, T. Weidner, N. Ballav and M. Zharnikov, *Langmuir*, 2008, 24, 12883-12891.
58. J. Noh, Y. Jeong, E. Ito and M. Hara, *J. Phys. Chem. C*, 2007, 111, 2691-2695.
59. T. Ishida, N. Choi, W. Mizutani, H. Tokumoto, I. Kojima, H. Azehara, H. Hokari, U. Akiba and M. Fujihira, *Langmuir*, 1999, 15, 6799-6806.
60. D. G. Castner, K. Hinds and D. W. Grainger, *Langmuir*, 1996, 12, 5083-5086.
61. I. A. Shkrob, T. W. Marin, Y. Zhu and D. P. Abraham, *The Journal of Physical Chemistry C*, 2014, 118, 19661-19671.